Electrochemical Recovery of Iron from Spent Pickle Liquor by Chloride-Based Molten Salt Electrolysis

To cite this article: Anar Badalbayli *et al* 2025 *ECS Adv.* **4** 043001

ECS Advances, 2025 **4** 043001

Electrochemical Recovery of Iron from Spent Pickle Liquor by Chloride-Based Molten Salt Electrolysis

Anar Badalbayli,[1,*] Nicholas Sinclair,[1,] Eunjeong Kim,[2] Alexander A. Baker,[2] and Rohan Akolkar[1,***,z]**

[1]*Department of Chemical and Biomolecular Engineering, Case Western Reserve University, Cleveland, Ohio 44106, United States of America*
[2]*Materials Science Division, Lawrence Livermore National Laboratory, Livermore, California 94550, United States of America*

Spent pickle liquor (SPL) is a waste stream generated in the steel industry that presents both a disposal challenge and a potential resource for metal recovery. This study investigates the electrochemical extraction of high-purity iron metal from SPL using chloride-based molten salt electrolysis (CMSE). Electrochemical characterization of diluted SPL confirmed Fe^{2+} as the dominant species. Thermal dehydration of SPL under inert atmosphere yielded $FeCl_2$-rich solids, which were directly employed as feedstock for electrolysis in LiCl–KCl eutectic melts at 500 °C. Cyclic voltammetry of $FeCl_2$ in this melt revealed well-defined Fe^{2+}/Fe^0 redox behavior within the electrochemical stability window of the supporting electrolyte. High coulombic efficiency (>85%) electrodeposition was achieved demonstrating that iron metal can be produced from dehydrated SPL by CMSE. The electrodeposited iron exhibited >98 wt% purity, which was further enhanced to 99.9 wt% via arc melting. The resulting iron powder was ferromagnetic, and its size distribution was found to be suitable for powder metallurgy applications. This work demonstrates a scalable, energy-efficient pathway for valorizing SPL into high-purity iron metal, advancing circular economy strategies in the steel industry.

 [DOI: 10.1149/2754-2734/ae114b]

Manuscript submitted August 7, 2025; revised manuscript received September 16, 2025. Published October 23, 2025.

The steel industry plays a foundational role in global infrastructure and manufacturing. Nearly 2 billion metric tons of steel are produced annually, enabling applications spanning construction, transportation, energy, and consumer goods.[1] To ensure the quality and performance of steel products, surface treatment through acid pickling is widely employed. This process removes oxide scales and rust formed during hot working operations, thereby preparing the steel surface for subsequent processing such as cold rolling, coating, or welding. The pickling process typically involves immersion of steel in dilute acid baths such as sulfuric acid, hydrofluoric acid, hydrochloric acid, or nitric acid. Among these, hydrochloric acid (HCl) is becoming the primary choice due to its effectiveness across various steel grades and surface finishing requirements.[2,3]

During pickling, the acid reacts with the oxide layer and the base iron metal, forming dissolved metal salts and gradually neutralizing the acid. As the concentration of dissolved metals increases, the efficiency of pickling declines, necessitating the disposal of the generated spent pickle liquor (SPL).[4–6] SPL is a corrosive, metal-rich waste stream containing residual free acid and dissolved salts of iron, chromium, copper, nickel, and zinc.[7] The volume of SPL generated is substantial, amounting to approximately 15–45 kilograms per ton of galvanized steel processed.[8,9] The accumulation of ferrous chloride and other metal salts in the bath renders it ineffective over time, and the disposal of SPL has posed a persistent environmental challenge for the steel industry.[4]

Currently, the most widely adopted SPL treatment methods involve chemical neutralization using alkaline reagents such as caustic soda, quicklime, liquid ammonia, or industrial by-products like carbide slag.[10,11] These agents precipitate metal hydroxides such as $Fe(OH)_3$, resulting in the formation of iron-rich sludge. While this approach is simple and effective in reducing immediate hazards, it suffers from significant drawbacks. Large quantities of neutralizing agents are required, and the resulting sludge presents a secondary solid waste management problem.[12,13] Moreover, these processes typically do not enable resource recovery, leading to the loss of valuable metals and reagents and incurring high costs associated with sludge disposal and environmental compliance.[14,15] The sludge itself is often of low value and must be landfilled, posing long-term risks to soil and groundwater due to eventual leaching of the heavy metals it contains.[12,14–16]

Alternative treatment methods have been explored in the literature, including membrane distillation,[17] selective precipitation,[18] anion exchange and membrane electrowinning,[19] and microbial oxidation followed by liquid–liquid extraction and solvothermal synthesis of ferrites.[16,17] While these approaches offer improved selectivity and potential for resource recovery, they are often limited by high operational costs, membrane fouling, and complexity in separating multiple metal species.[5,20] Solvent extraction, for instance, has been used to selectively separate zinc and iron from mixed-acid SPL, but challenges such as phase separation, solvent degradation, and economic feasibility remain unresolved.[21] The dual nature of SPL as both an environmental liability and as a potentially valuable secondary resource has recently stimulated research into alternative approaches aimed at valorizing SPL.

Electrochemical treatment of SPL has long been a subject of industrial and academic interest, with early innovations dating back to the early 20th century.[22–25] These foundational efforts focused on recovering metallic iron and regenerating acids from SPL generated during steel pickling operations. Mainly, acid regeneration remained the central focus of studies that explored membrane-based separation and electro-membrane processes for reclaiming pickling acid and reducing hazardous waste volume.[26,27] Over time, the scope of this research broadened to include selective metal recovery, synthesis of industrially valuable compounds, and integration of SPL treatment into industrial circular economy frameworks. Recent studies have demonstrated the electrochemical synthesis of high-purity magnetite (Fe_3O_4),[28,29] selective separation of zinc and iron using membrane electrowinning and ion exchange,[30,31] and conversion of SPL into advanced materials such as battery-grade metal oxides.[32] Process optimization techniques, including ultrasonic-assisted extraction, have further improved efficiency and selectivity.[29,33] This evolution reflects a shift from basic acid recovery toward comprehensive resource valorization, positioning electrochemical SPL treatment as a key strategy for achieving efficiency in steel manufacturing. By enabling the recovery of iron and regeneration of HCl, electrochemical

*Electrochemical Society Student Member.
**Electrochemical Society Member.
***Electrochemical Society Fellow.
[z]E-mail: RNA3@case.edu

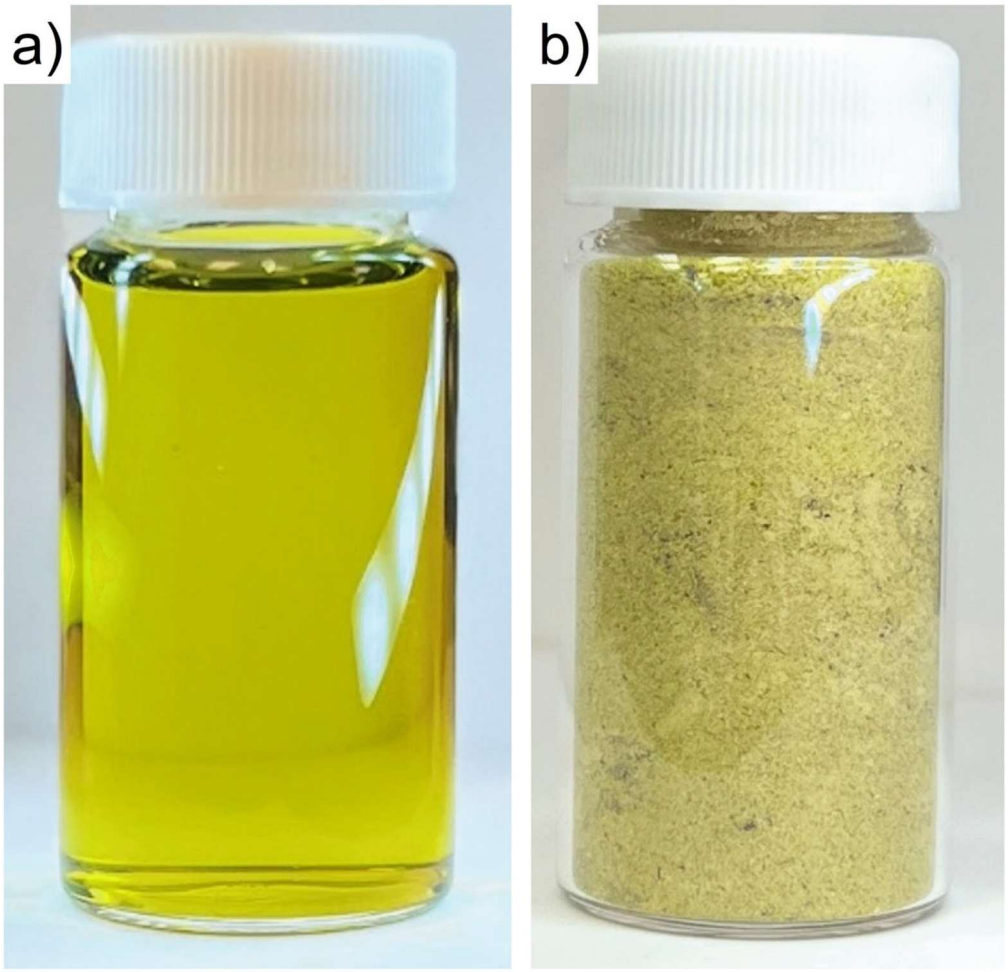

Figure 1. Spent pickle liquor (SPL) as-received (a) and after dehydration at 150 °C under inert argon (b). The dried solid phase of SPL in (b) was then subjected to CMSE.

processes have the potential to close the loop in steel pickling operations, reducing reliance on raw materials and minimizing environmental impact. However, widespread adoption of these technologies requires further investigation into process optimization, scalability, and integration with existing industrial workflows.

This study aims to evaluate the feasibility of electrochemical recovery of iron from SPL, with particular emphasis on chloride-based molten salt electrolysis as a promising route for converting industrial waste into high-purity metal. Building on previous work that demonstrated the effectiveness of CMSE for iron recovery from ore-based feedstocks,[34] this study explores the use of dehydrated SPL as an industrial waste feedstock for CMSE. We show here that CMSE enables iron electrowinning at high current densities, yielding compact and ferromagnetic metal with minimal contamination (>99 wt% pure Fe). By integrating SPL valorization with CMSE, the work contributes to economically-sustainable steel manufacturing and circular economy strategies, offering a scalable pathway for resource recovery and waste minimization.

Experimental Methods

Aqueous SPL analysis.—As-received SPL obtained from a local steel plant (courtesy Cleveland Cliffs Inc.) was diluted 20-fold in 0.1 M HCl (Thermo Scientific) for electrochemical experiments. Cyclic voltammetry (CV), slow-scan linear sweep voltammetry (LSV) and chronoamperometry were performed on the diluted SPL at ambient temperature using a Gamry Interface 1010E potentiostat. A 5 mm diameter platinum (Pt) rotating disk electrode (RDE) was used as the working electrode, a Pt wire was used as the counter electrode, and a Ag/AgCl (3 M KCl) electrode served as the reference electrode. CV scans were performed at a scan rate of 50 mV s^{-1}. LSV measurements were conducted at 10 mV s^{-1} scan rate, with RDE rotation speeds ranging from 800 to 1800 rpm. Chronoamperometry was conducted at a fixed potential of 1.1 V vs Ag/AgCl.

Thermal dehydration of SPL.—The SPL was dried under flowing argon at 150 °C until visible evaporation of moisture and solvent was noticed (Fig. 1). The resulting solid product was ground into a fine powder and stored in sealed containers under an inert atmosphere to prevent oxidation and re-hydration. Material characterization was performed using scanning electron microscopy (SEM, Apreo, Thermo Fisher Scientific) and energy-dispersive X-ray spectroscopy (EDS) to assess morphology and elemental composition.

CMSE experiments.—Molten salt electrolysis setup was located inside an argon-filled glovebox with moisture levels maintained below 300 ppm. Oxygen concentration in the glovebox was not directly measured. The electrochemical cell was a borosilicate glass Berzelius beaker (US Plastic Corp.), operated at 500 °C by placing it inside an electric furnace (VEVOR GF1100ND3). Both the working and counter electrodes were finely extruded graphite rods (Graphite Store) with a 0.25 inch diameter. The reference electrode was a custom-fabricated Ag/Ag^{+} electrode consisting of Ag wire immersed in LiCl–KCl with 1 wt% AgCl, housed in a 5 mm NMR tube. The

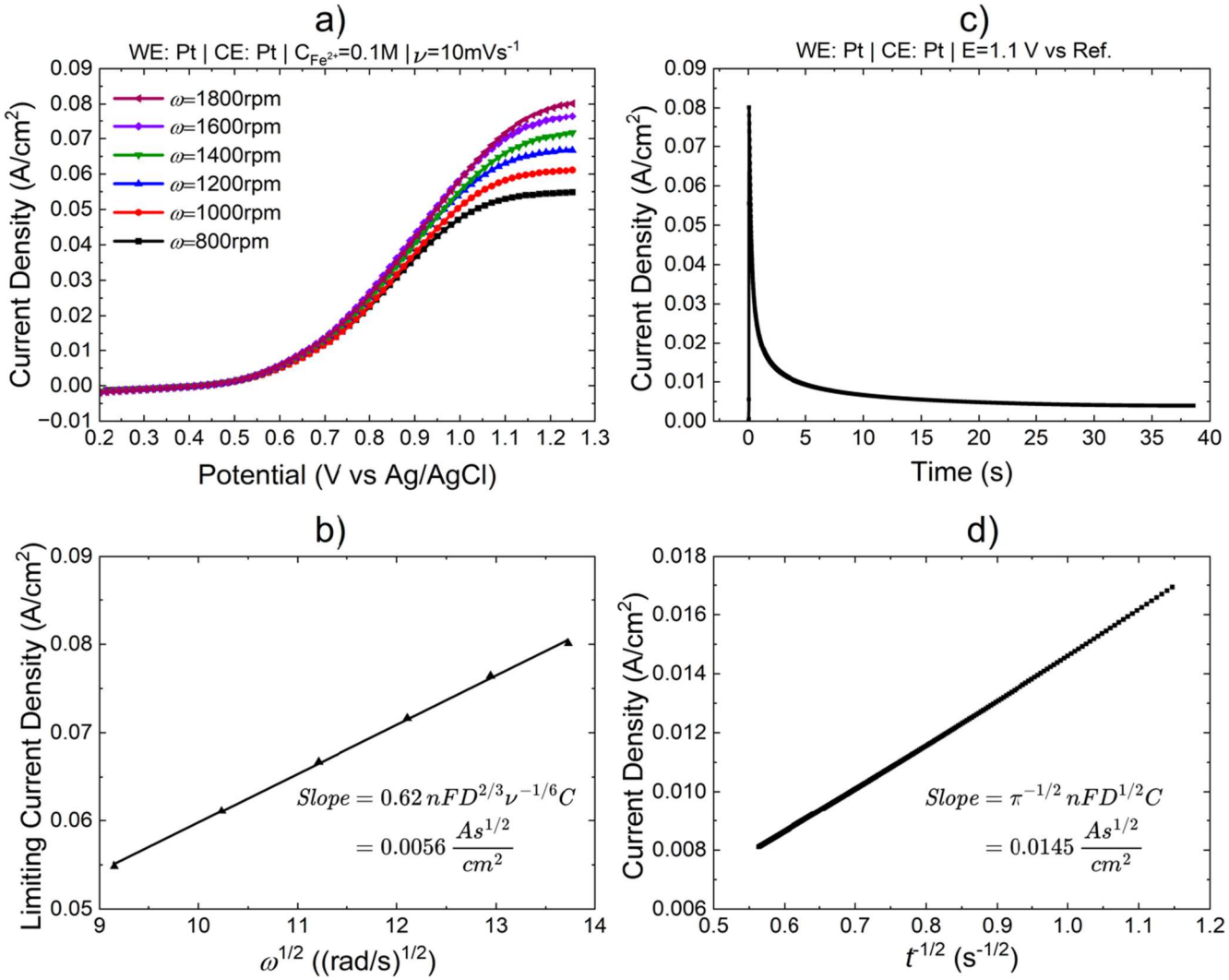

Figure 2. Electrochemical analysis of 20x diluted SPL solution on a Pt RDE. (a) The slow-scan LSV curves recorded at rotation rates ranging from 800 to 1800 rpm. (b) Levich plot of limiting current densities from (a) as a function of the square root of rotation rate ($\omega^{1/2}$), yielding a linear relationship. (c) Chronoamperometry conducted at a fixed potential of 1.1 V vs Ag/AgCl in 20x diluted SPL on a disk electrode at 0 rpm. (d) Cottrell analysis of data from (c). Slopes in (b) and (d) yielded the Fe^{2+} concentration and its diffusivity in SPL.

cell design and setup have been described previously.[34] $FeCl_2$ was introduced to the melt at a concentration of 50 mM using one of three sources: anhydrous $FeCl_2$ (Sigma-Aldrich, 99.9%), $FeCl_2{\cdot}4H_2O$ (Sigma-Aldrich), and dehydrated SPL powder prepared per procedure described above. Electrochemical measurements, CV, electrochemical impedance spectroscopy (EIS), galvanostatic deposition (at 25 mA cm^{-2} for 15 s), and stripping coulometry (at 0.5 V vs Ag/Ag$^+$), were performed using a Gamry Interface 5000E potentiostat. EIS was carried out potentiostatically at open-circuit potential over a frequency range 1 Hz–1 MHz, and the high-frequency resistance was used for IR_Ω compensation. Electrodeposited Fe samples were arc melted using an arc melter (Edmund Buehler MAM-1) under an argon atmosphere. To ensure complete removal of entrapped salts, the Fe bead was re-melted also under an argon atmosphere. The bead surfaces were polished by ion beam milling (EM TIC 3X, Leica Microsystems), and the interior regions were analyzed by SEM and EDS (Apreo, Thermo Fisher Scientific). Particle size distribution of the electrowon iron powder was measured using laser diffraction in an aqueous suspension, employing Mie theory that models light scattering by spherical particles, used to determine particle size distribution and adaptive volume-based analysis mode which adjusts for particle shape and refractive index to improve accuracy in heterogeneous samples (Bettersize Instruments Ltd.).

Results and Discussion

Electrochemical characterization of spent pickle liquor.— Electrochemical characterization of spent pickle liquor (SPL, diluted 20x) was conducted using a combination of rotating disk electrode (RDE) voltammetry and chronoamperometry. Figure 2a shows linear sweep voltammetry (LSV) data collected using a Pt working electrode at various rotation rates (800–1800 rpm). With increasing rotation speed, the limiting current density associated with the reaction $Fe^{2+} \rightarrow Fe^{3+} + e$ increases, confirming that the electrochemical reaction experiences diffusion-limitations at large anodic overpotentials. At 1800 rpm, the limiting current was approached but not fully reached, with a slight upward drift beyond 1.2 V. For consistency across all rotation rates, the limiting current density was taken at 1.2 V. The dependence of limiting current on the square root of the rotation rate was further analyzed (Fig. 2b), which shows a linear relationship in accord with the Levich equation:[35]

$$i_L = 0.62nFD^{\frac{2}{3}}\nu^{-\frac{1}{6}}C\omega^{\frac{1}{2}} \quad [1]$$

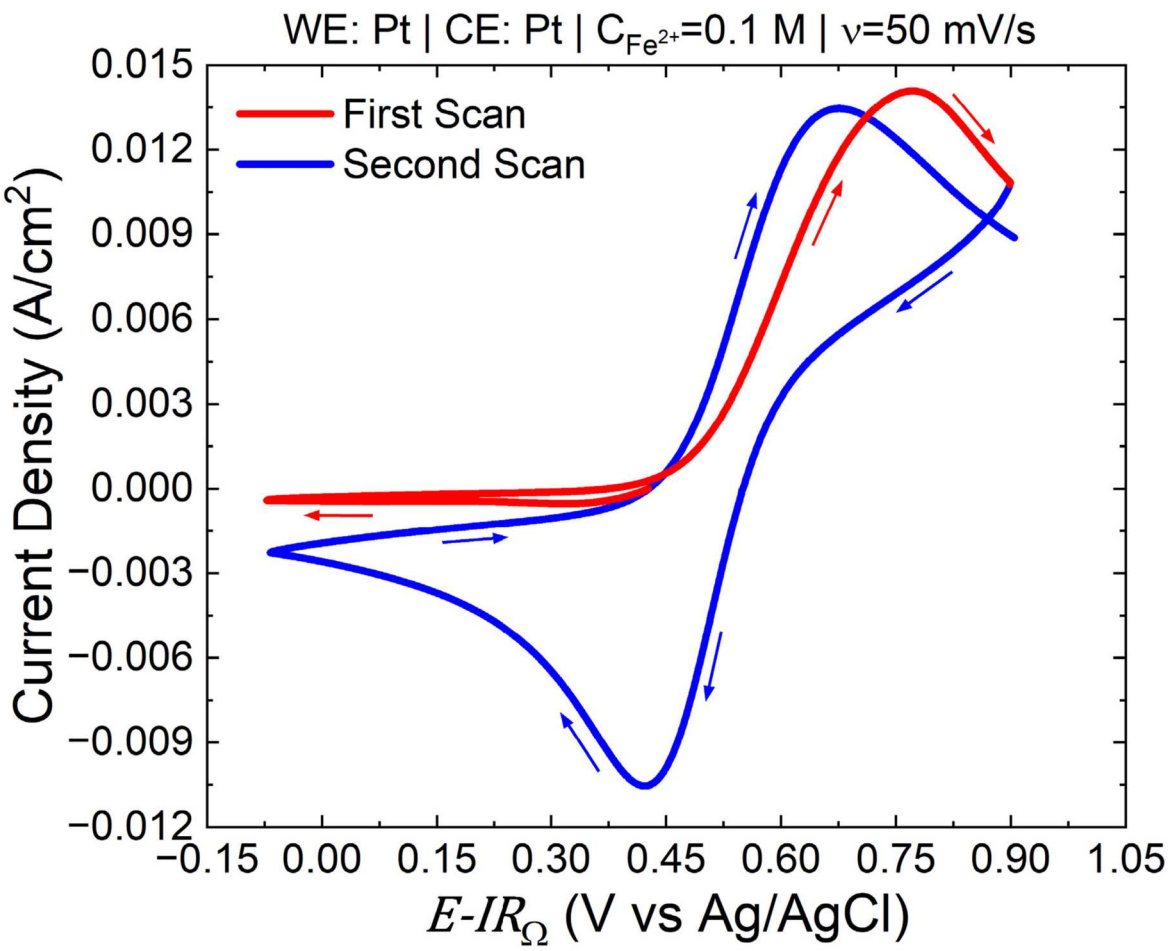

Figure 3. Cyclic voltammogram of 20x diluted SPL recorded at room temperature on a Pt WE at a scan rate of 50 mV s^{-1}. First scan shows absence of Fe^{3+} reduction wave, indicating that as-received SPL predominantly contains Fe^{2+}.

where i_L is the limiting current density, n is the number of electrons transferred (=1 for Fe^{2+} oxidation), F is the Faraday's constant, D is the diffusion coefficient, ν is the kinematic viscosity of the electrolyte (0.01 cm^2 s^{-1}) which is assumed based on dilute solution of chloride salts,[36] C is the bulk concentration of Fe^{2+}, and ω is the angular rotation rate. In this analysis, one-electron anodic oxidation ($Fe^{2+} \rightarrow Fe^{3+} + e$) was considered since this provides a well-defined framework for extracting diffusivity and concentration values of Fe^{2+} from RDE data. The slope of the linear fit in Fig. 2b was measured and found to be:

$$0.62nFD^{\frac{2}{3}}\nu^{-\frac{1}{6}}C = 0.0056\ \frac{As^{\frac{1}{2}}}{cm^2} \qquad [2]$$

Chronoamperometry was also performed at a fixed applied potential of 1.1 V vs Ag/AgCl, as shown in Fig. 2c. The transient current decay observed is typical of diffusion-controlled Fe^{2+} oxidation. Plotting the current density against $t^{-1/2}$ (Fig. 2d) yields a straight line, consistent with the Cottrell equation, with slope of:

$$\pi^{-\frac{1}{2}}nFD^{\frac{1}{2}}C = 0.0145\frac{As^{\frac{1}{2}}}{cm^2} \qquad [3]$$

Equations 2 and 3 can be solved to determine the two unknowns, i.e., the diffusion coefficient and the concentration of Fe^{2+} in the diluted spent pickle liquor. Values determined were: $D = 6.5 \times 10^{-6}$ cm^2/s and $C = 0.1$ M, respectively. These values are consistent with literature-reported diffusion coefficients for Fe^{2+} in chloride melts, which typically are in the 10^{-6}–10^{-5} cm^2 s^{-1} range, depending on the ionic strength and the supporting electrolyte composition. The determined concentration C aligns well with that expected for typical SPL after 20-fold dilution,[19] based on which we can conclude that the actual Fe^{2+} concentration in the as-received spent pickle liquor was around 2 M.

Relative concentrations of Fe^{2+} and Fe^{3+} in spent pickle liquor.—Figure 3 shows cyclic voltammetry (CV) performed on the diluted SPL to investigate its redox behavior and to determine the relative concentrations of Fe^{2+} and Fe^{3+} in it. CV measurement was performed at room temperature using platinum working and counter electrodes, and at a scan rate of 50 mV s^{-1}. In the first scan, there is no distinct cathodic peak observed in the negative scan direction indicating that Fe^{3+} was largely absent in the starting solution. Notably, a clear anodic peak appears during the positive scan direction around 0.75 V vs Ag/AgCl, corresponding to the oxidation of Fe^{2+} in SPL to Fe^{3+}. In the second scan, however, both a prominent cathodic peak (reduction of Fe^{3+} back to Fe^{2+} at around 0.42 V vs Ag/AgCl) and a subsequent anodic peak are observed. The appearance of the reduction peak in the second scan confirms that Fe^{3+} was generated electrochemically during the first oxidative sweep and was not present initially in the diluted SPL solution. The current density ratio of the oxidation and reduction peaks (1st scan) indicate a Fe^{2+}/Fe^{3+} ratio of approximately 20:1 in SPL. This confirms that the spent pickle liquor, as received or diluted, consisted predominantly of Fe^{2+} species. The predominance of $FeCl_2$ over $FeCl_3$ is typical for hydrochloric acid pickling baths.[21] The electrochemical behavior observed in CV supports the earlier concentration analysis (Fig. 2) and provides additional evidence that the SPL feedstock is well-suited for efficient conversion to dehydrated $FeCl_2$ via thermal treatment.

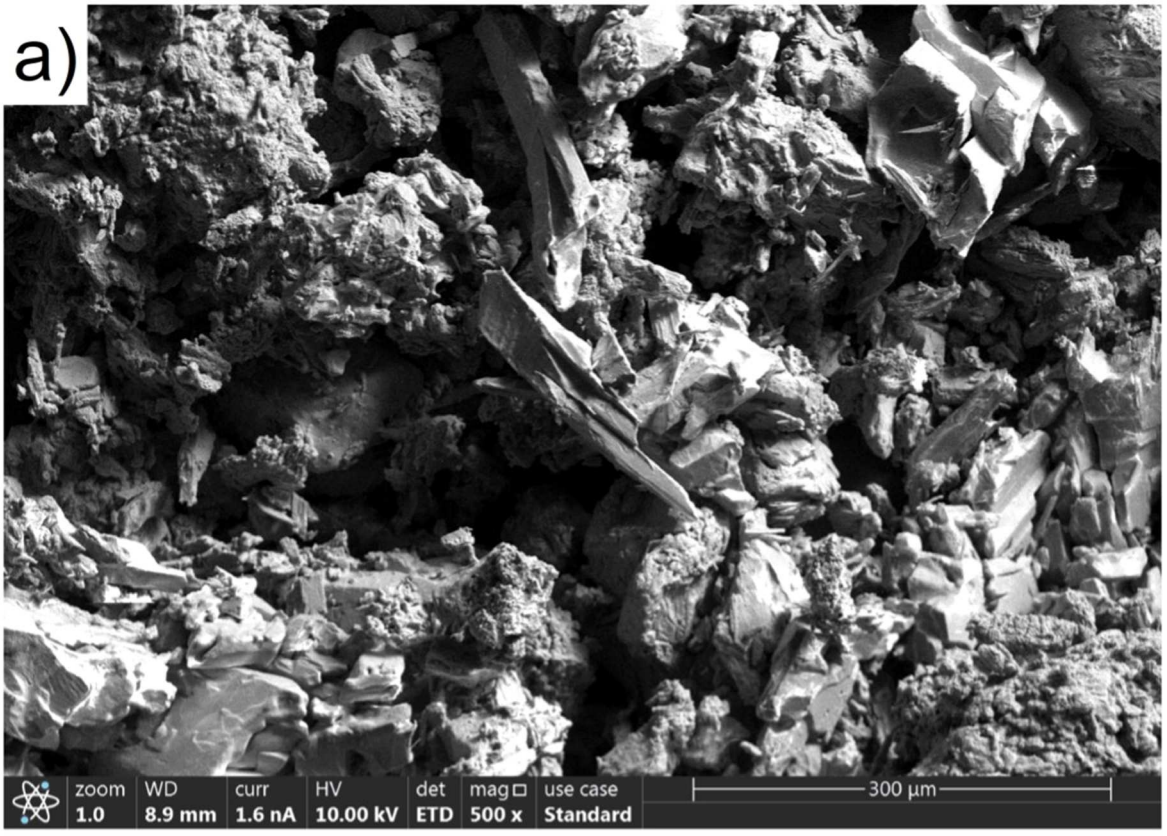

b)

	O	Ni	Al	Cl	Fe
Weight %	2.00	0.20	0.20	54.90	42.80
Atom %	5.10	0.10	0.30	63.20	31.30

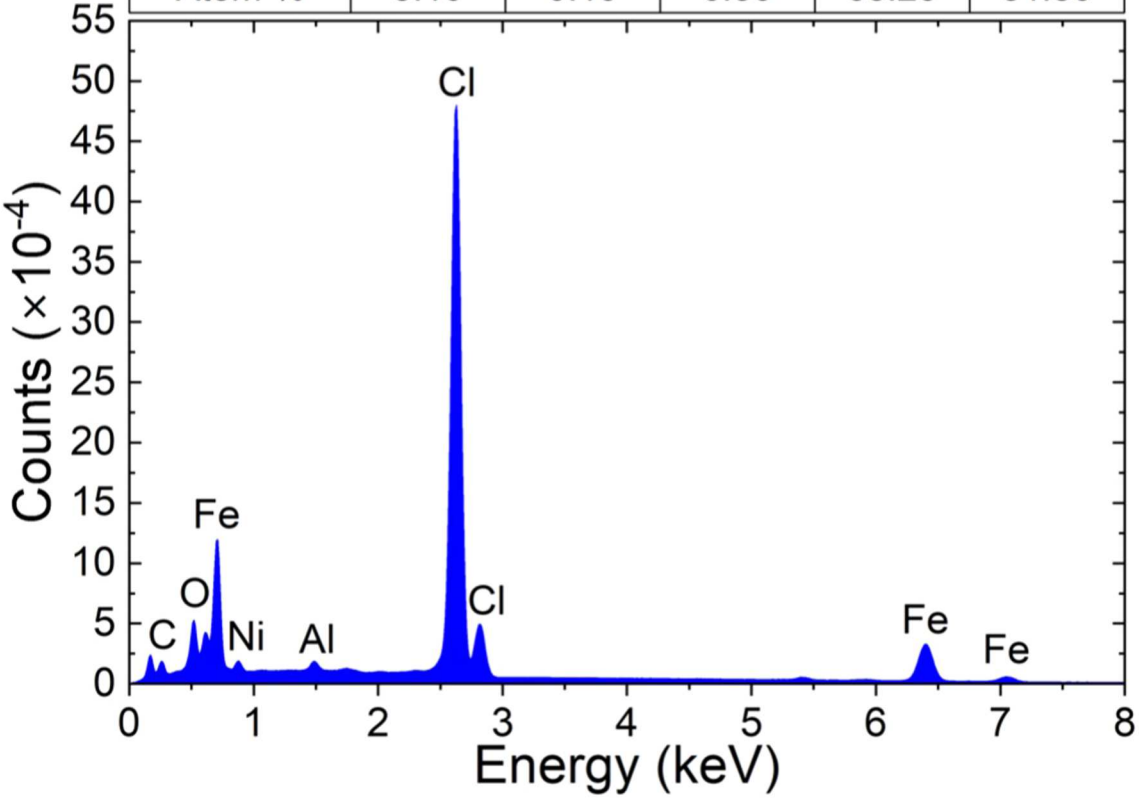

Figure 4. Characterization of dehydrated SPL. (a) SEM image of dehydrated SPL from Fig. 1b, and (b) Corresponding EDS analysis, revealing that the dehydrated SPL is predominantly composed of Fe and Cl in a 1:2 atomic ratio suggesting it comprises mainly of $FeCl_2$.

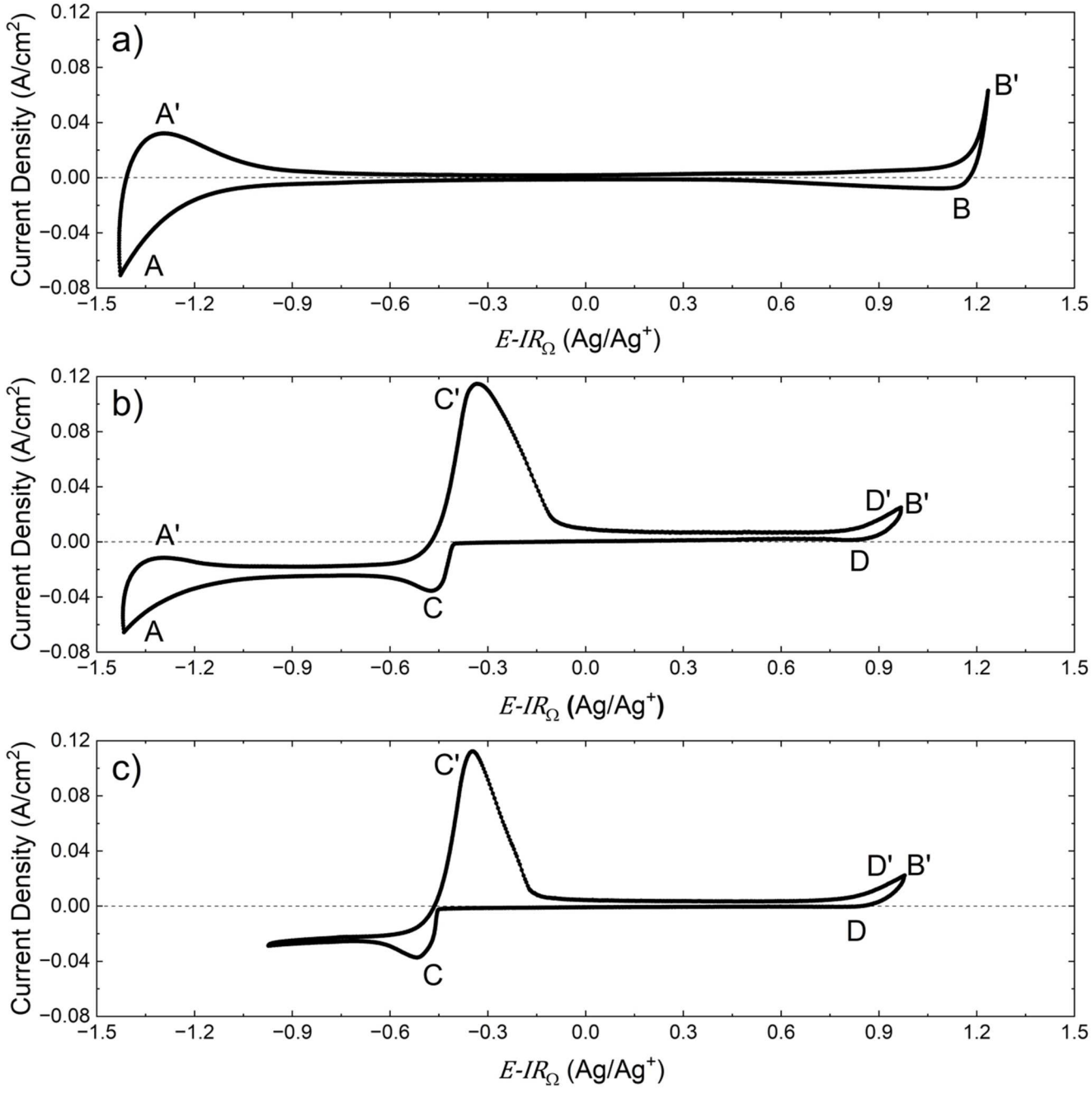

Figure 5. Cyclic voltammograms (CV) in LiCl–KCl eutectic (45:55 wt%) at 500 °C using a graphite working electrodes (surface area = 2 cm^2) at a scan rate of 100 mV s^{-1}. (a) CV of the neat electrolyte, showing an electrochemical stability window of approximately 2.4 V. (b) CV after addition of 50 mM dehydrated SPL, revealing two redox transitions: Fe^{3+}/Fe^{2+} near +1.0 V and Fe^{2+}/Fe^{0} near –0.45 V vs Ag/Ag$^+$. (c) Same as (b), but with a vertex potential of –1.0 V vs Ag/Ag$^+$.

Thermal dehydration of spent pickle liquor and subsequent CMSE.—To prepare SPL for molten salt electrolysis, the as-received SPL solution was dehydrated under inert (Ar) atmosphere at 150 °C to avoid oxidation of Fe^{2+} to Fe^{3+} during heating. Figure 4a depicts a scanning electron microscopy (SEM) image of the resulting solid product, while Fig. 4b shows the corresponding energy-dispersive X-ray spectroscopy (EDS) and quantitative elemental analysis of the sample. The morphology captured in the SEM image reveals a mixture of plate-like crystallites, commonly seen in dehydrated metal chloride salts.[37] EDS spectrum confirms that the dehydrated SPL is primarily composed of iron (Fe) and chlorine (Cl), with Fe and Cl amounting to 42.80 wt% and 54.90 wt%, respectively. The atomic percentages (Fe 31.30%; Cl 63.20%) are also generally consistent with the expected stoichiometry and oxidation state of iron in $FeCl_2$, validating again that the predominant species in the dehydrated product is $FeCl_2$. This observation aligns with the electrochemical data presented in Fig. 3, which indicated a strong prevalence of Fe^{2+} over Fe^{3+} in the as-received SPL, and that this ratio is preserved even after dehydration. Small amounts of aluminum (Al) and nickel (Ni) were also detected in dehydrated SPL, with each contributing $<$0.2 wt%. These elements are likely present as trace contaminants originating from alloying elements in steel scrap or from corrosion of stainless steel components during acid pickling. Such impurities are commonly reported in industrial SPL, and have been detected in similar studies involving acid regeneration processes from pickling baths.[38] The small oxygen

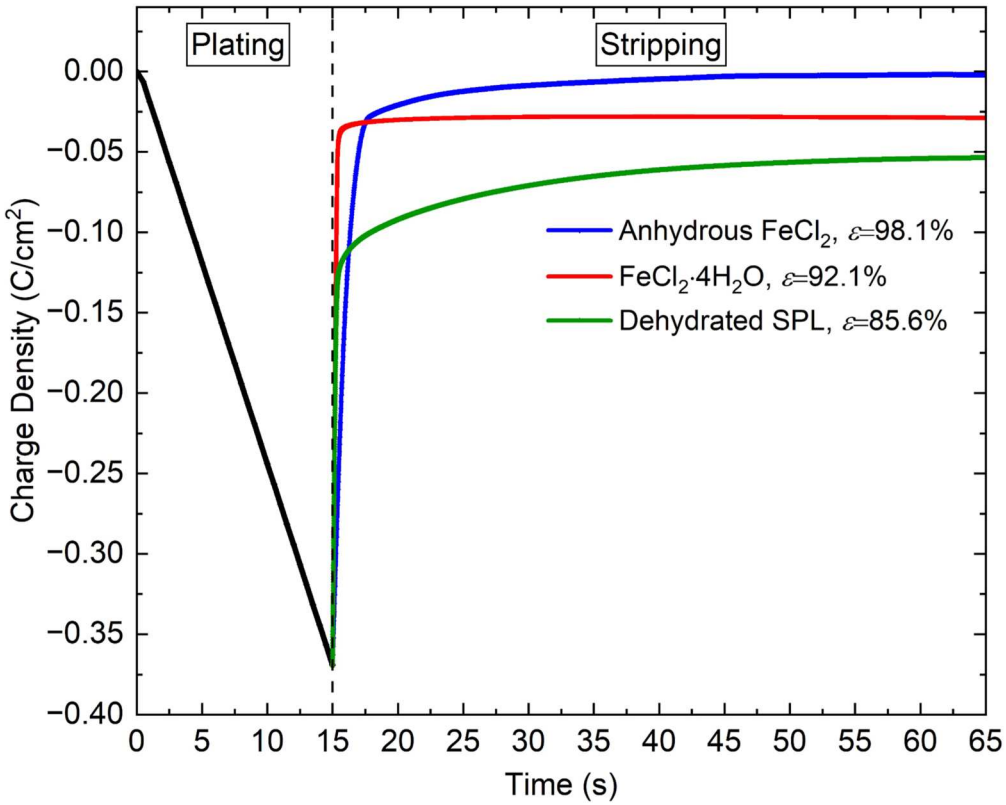

Figure 6. Coulombic efficiency measurements for iron deposition during CMSE. Stripping coulometry involved galvanostatic plating (for 15 s at 25 mA cm^{-2}), followed by anodic stripping at 0.5 V vs Ag/Ag^{+}. Anhydrous $FeCl_2$ exhibits the highest Coulombic efficiency (98.1%), followed by $FeCl_2{\cdot}4H_2O$ (92.1%), and then dehydrated SPL (85.6%), highlighting the influence of hydration on deposition efficiency.

signal observed is attributed either to surface oxidation during sample handling or trace moisture in the sample chamber but does not indicate bulk Fe^{3+} formation. The crystalline nature of the dried salt product, its stoichiometry suggestive of $FeCl_2$, and high purity support its use as a suitable feedstock for the next stage of processing, i.e., metallization to Fe via chloride-based molten salt electrolysis (CMSE).

Electrochemical behavior of dehydrated SPL in LiCl–KCl melts.—Electrochemical response of dehydrated spent pickle liquor in the molten salt was examined using voltammetry on a graphite working electrode at 500 °C in an LiCl–KCl eutectic melt (45–55 wt%). Figure 5a shows the CV of the neat eutectic LiCl–KCl electrolyte. The voltammogram reveals a broad electrochemical stability window of approximately 2.4 V, defined by the onset of alkali metal (Li/K) plating around –1.2 V vs Ag/Ag^{+} (peak A) and chlorine gas evolution at +1.2 V (peak B′). The corresponding stripping (A′) and reduction (B) currents are relatively low due to the physical detachment of liquid alkali metal droplets and diffusive escape of Cl_2 gas, respectively—both are well-documented phenomena in molten chloride electrolysis.[34] In Fig. 5b, the introduction of dehydrated SPL (at 50 mM Fe^{2+} when added to the melt) results in new electrochemical features, particularly a pair of redox peaks at –0.47 V and –0.33 V vs Ag/Ag^{+} (C/C′), corresponding to the $Fe^{2+} + 2e \leftrightarrow Fe^{0}$ couple. The anodic peak near +1.0 V (D) corresponds to $Fe^{2+} \rightarrow Fe^{3+}$ oxidation, while the cathodic peak near –0.33 V (C′) is assigned to re-oxidation of Fe^{0} formed at –0.47 V (C) back to Fe^{2+}. This again confirms that $FeCl_2$ is the primary electroactive species present after dehydration, and after dissolution in the melt. As expected, the Fe reduction potential lies within the electrochemical stability window of the LiCl–KCl melt, in agreement with literature reports.[39–41] This suggests that efficient and selective electrodeposition of iron metal from the dehydrated SPL is feasible in the chloride molten salt without significant interference from parasitic reactions. Figure 5c presents a CV collected under the same conditions, but with the vertex potential limited to –1.0 V vs Ag/Ag^{+} to better isolate the Fe^{2+}/Fe^{0} redox couple. The anodic and cathodic peaks remain well-defined, confirming accessibility of Fe^{2+} in the SPL-derived feed for Fe metal electro-synthesis.

Coulombic efficiency of Fe deposition from SPL-derived Fe^{2+} in LiCl–KCl molten salts.—Iron electrodeposition efficiency was measured when plating from three different electrolytes: 50 mM anhydrous $FeCl_2$, $FeCl_2{\cdot}4H_2O$, and dehydrated spent pickle liquor, all in the LiCl–KCl eutectic molten salt as supporting electrolyte at 500 °C. For measuring efficiency, stripping coulometry (Fig. 6) was employed in which galvanostatic plating (at 25 mA cm^{-2}) for 15 s was followed by stripping under potentiostatic conditions (at 0.5 V vs Ag/Ag^{+}), with the charge density monitored over time. Coulombic efficiency was calculated by comparing the integrated stripping charge to the plating charge passed, representing the fraction of deposited iron that is reversibly recovered as Fe^{2+}. The efficiency for 50 mM anhydrous $FeCl_2$ reached 98.1%, consistent with literature reports showing that high-purity $FeCl_2$ is an ideal precursor for molten salt electrolysis of iron, yielding compact, adherent deposits and minimal parasitic reactions.[40] The absence of water or oxidized (Fe^{3+}) species ensures that nearly all of the applied current contributes to the desired plating reaction. In contrast, 50 mM $FeCl_2{\cdot}4H_2O$ shows a slightly lower coulombic efficiency of 92.1%. The reduced efficiency likely arises from residual water of hydration which can interfere with the molten salt electrochemistry by introducing side reactions such as hydrogen evolution and $FeCl_2$ sublimation and decomposition, ultimately decreasing the coulombic efficiency.[42,43] The dehydrated SPL, while showing the lowest coulombic efficiency (85.6%), still demonstrates excellent electrochemical activity and practical viability for iron recovery. The lower coulombic efficiency can be attributed to the complex composition of SPL, which contains trace impurities (e.g., Ni, Al, O) and potential

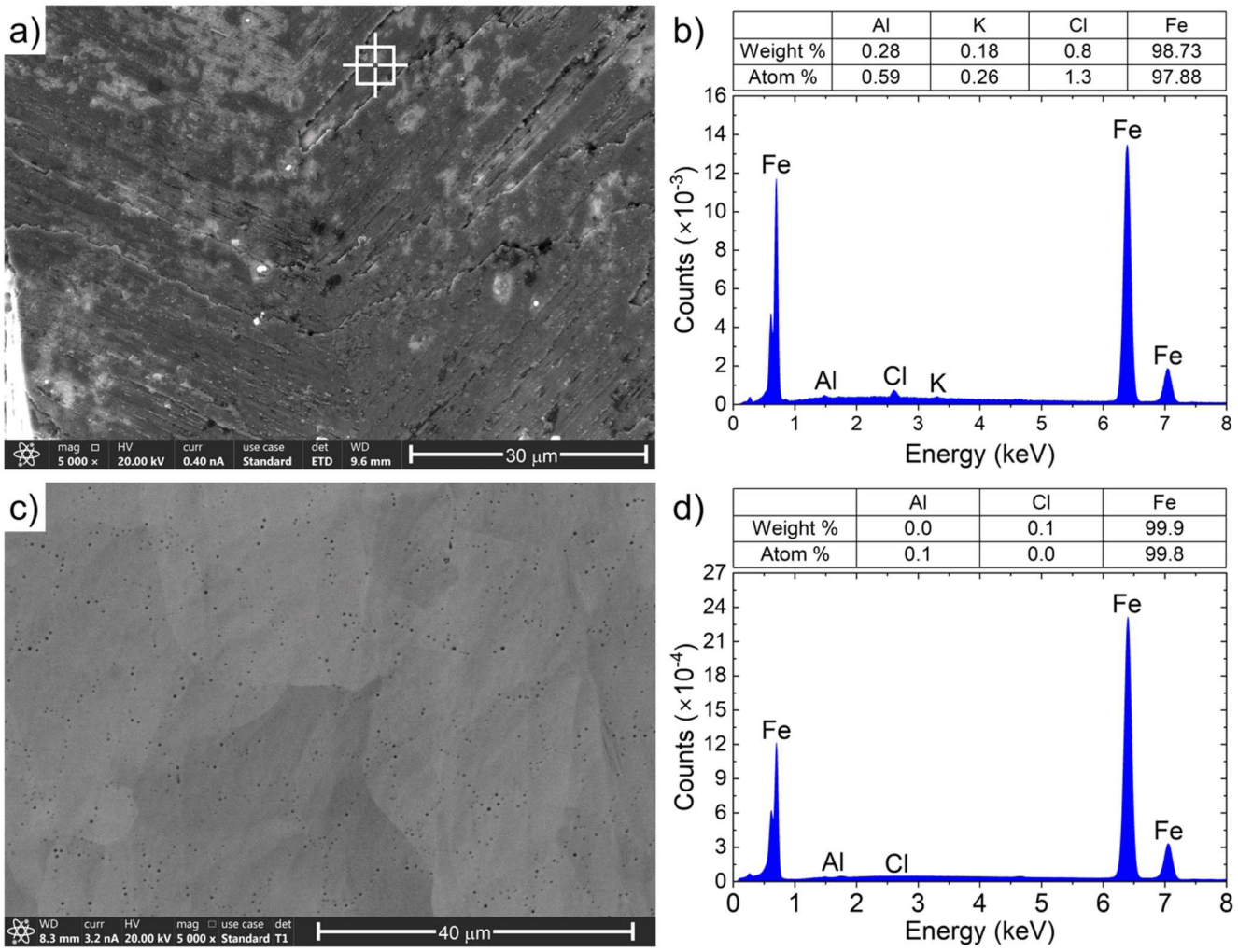

Figure 7. Morphology and purity analysis of electrowon iron obtained via CMSE of dehydrated SPL. (a) SEM image of as-deposited iron, showing a rough surface morphology. (b) Spot EDS analysis of the area indicated in (a), revealing 98.73 wt% Fe with minor impurities. (c) SEM image of the same sample in (a) but after arc re-melting, exhibiting a dense, homogeneous microstructure with visible micro-voids attributed to salt evaporation. (d) Area EDS of the region in (c), confirming increased purity to 99.9 wt% Fe post arc re-melting.

residual moisture or oxidized Fe^{3+} species even after dehydration in vacuum or in an inert atmosphere. These components may lead to parasitic current loss via side reactions or irreversible iron precipitation. Nevertheless, the fact that efficiency remains above 85% is significant, confirming that the SPL-derived dehydrated $FeCl_2$ is sufficiently pure for energy-efficient CMSE without the need for extensive purification or pretreatment. Moreover, this efficiency result compares favorably with other industrial-grade feedstocks investigated in high-temperature electrochemical processes.[44] The marginal loss in efficiency may be acceptable in large-scale industrial operations, especially when weighed against the benefits of converting hazardous SPL waste into a functional feedstock for metal recovery.

Morphology and purity of Fe deposits obtained from SPL via CMSE.—Figure 7 presents the morphological and compositional characterization of Fe metal obtained via CMSE of dehydrated $FeCl_2$ (from SPL) added to a LiCl–KCl eutectic molten salt at 500 °C. Figure 7a is an SEM image of the Fe deposit collected on a graphite rod working electrode at a current density of 0.5 A cm^{-2}. The as-deposited Fe exhibits growth patterns and localized inhomogeneities —features often associated with high rate electrodeposition in molten salt media.[45] The large surface roughness is consistent with previous reports on CMSE of transition metals, particularly under mass-transfer-limited conditions and non-uniform current distribution.[34,46] EDS spot analysis at the highlighted point in Fig. 7a is presented in Fig. 7b. The deposit is composed of 98.73 wt% iron, with trace levels of chlorine (0.8 wt%) and very low levels of Al and K impurities, likely originating from the molten salt itself or from residual SPL constituents. Although Ni has a more positive standard reduction potential than Fe, its concentration in SPL was 0.1 at% and thus orders of magnitude lower than Fe. This disparity likely explains why Ni was effectively excluded during electrodeposition. While trace impurities such as Ni and Al did not co-deposit under the studied conditions, accumulation of non-ferrous species in the molten salt over time could require impurity management strategies. The atomic percentage of Fe (97.88%) confirms high purity of the deposited metal. Small inclusions of chloride salts may account for the remaining constituents of the iron deposits. Importantly, no nickel or other transition metals from SPL impurities were detected, suggesting effective exclusion during electrodeposition. To improve compactness and purity, the as-deposited iron was subjected to arc melting under an inert atmosphere. Figure 7c displays an SEM image of the arc-melted Fe, revealing a homogeneous and dense microstructure. The uniformly distributed dark spots seen are attributed to salt evaporation-induced porosity, a common feature in vacuum-arc or inert-atmosphere remelting processes.[47] This microstructure is favored for its mechano-thermal stability and indicates successful consolidation. Full-area EDS analysis of the arc-melted bead (Fig. 7d) shows that the re-melted

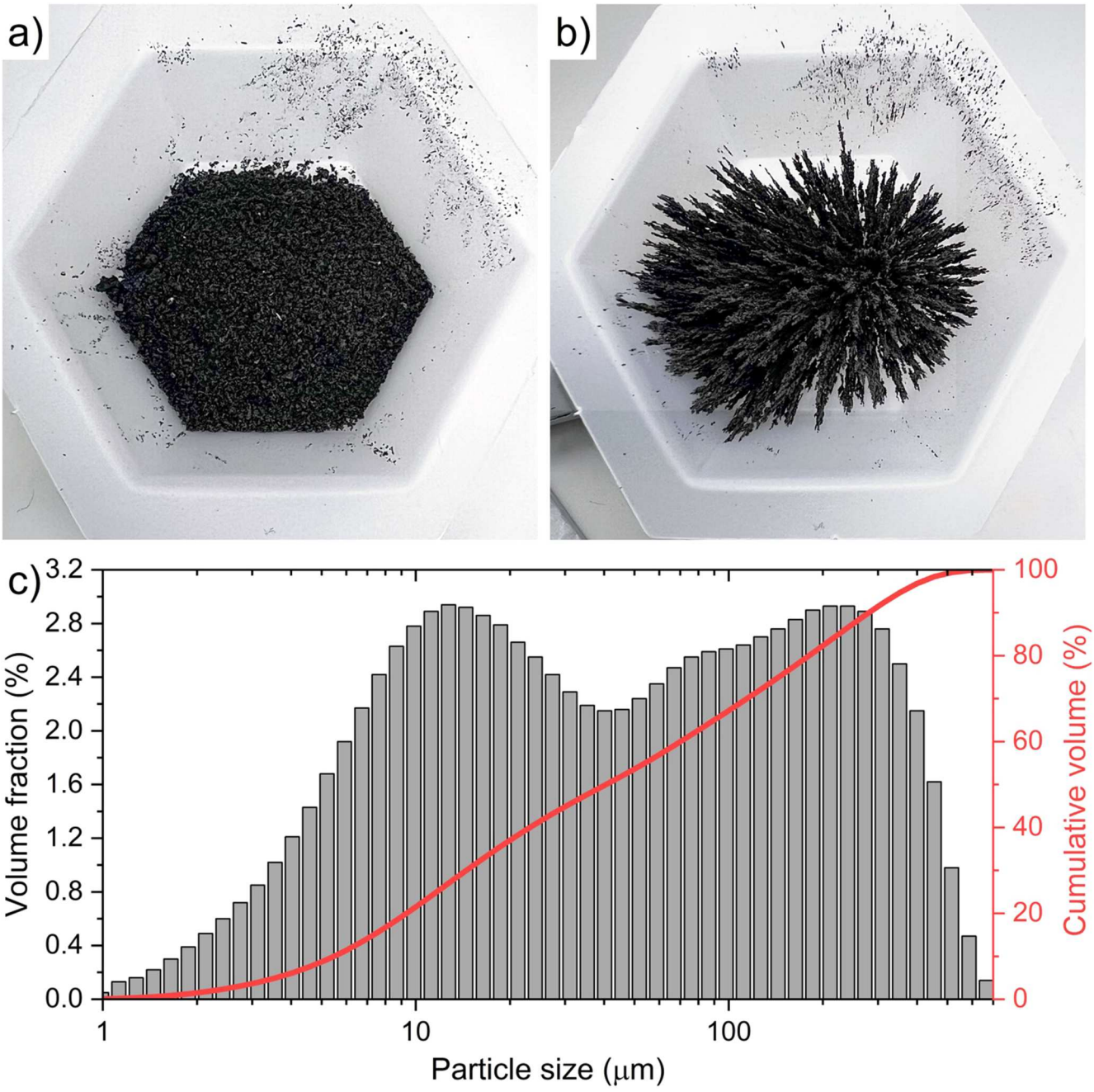

Figure 8. Iron electrowon using CMSE from a 2.5 M dehydrated SPL-containing LiCl–KCl melt at 500 °C and a current density of 0.5 A cm^{-2}. (a) Optical image of the electrowon iron powder obtained after CMSE and after purification via vacuum distillation at 1000 °C for 30 min. (b) The resulting iron powder exhibits magnetic response when exposed to a permanent magnet, confirming ferromagnetic behavior. (c) Particle size distribution of the electrowon iron powder.

deposit contains 99.9 wt% Fe, with only trace Cl (0.1 wt%) and no detectable Al or K. This dramatic reduction in residual contaminants underscores the effectiveness of arc melting in refining the electrodeposited Fe and removing adsorbed or trapped salts. Such purification strategies are routinely used in electrometallurgy to upgrade the electrowon metal quality for subsequent industrial use.[48] Overall, these results demonstrate that high-purity iron metal can be recovered directly from SPL via CMSE, and that minor surface contamination from chloride or impurities can be efficiently eliminated by post-electrolysis steps such as arc melting.

Particle size distribution of electrowon Fe powder.—Figure 8 characterizes the iron powder obtained following CMSE of dehydrated spent pickle liquor (2.5 M) at 0.5 A cm^{-2} current density, and subsequent vacuum distillation at 1000 °C for 30 min. Faradaic efficiency during bulk electrolysis at 0.5 A cm^{-2}, based on mass of Fe recovered, was ∼85%. This value is consistent with the short-term stripping coulometry results, demonstrating reproducibility over longer electrolysis time periods. The post-treatment step is effective, similar to arc re-melting, for removing residual chloride salts from the electrodeposited iron, which ensures high purity Fe powder recovery. The resulting product was analyzed for morphological features, magnetic behavior, and particle size distribution. Figure 8a shows Fe powder collected after vacuum distillation. The Fe powder is metallic gray and is free-flowing, suggesting successful removal of LiCl and KCl entrapped salts. These salts have high vapor pressure at elevated temperatures and are effectively removed via vacuum distillation.[49] We have previously demonstrated feasibility of this method for Fe powder purification.[34] Electrowon Fe powder when exposed to a permanent magnet (Fig. 8b) demonstrates magnetic

alignment, confirming its strong ferromagnetic properties. This behavior is characteristic of elemental Fe and further verifies that the recovered powder retains metallic identity after vacuum distillation. This also suggests that no significant oxidation occurred during post-electrolysis processing.[50] Figure 8c presents particle size distribution analysis of the powder. The distribution shows iron powder having a broad size range of 50–300 μm, with a peak distribution density between 200–250 μm. The cumulative distribution curve shows that approximately 90% of the particles fall below ∼250 μm. This relatively broad size distribution is also typical of high-temperature electrodeposition followed by mechanical disintegration or handling and is consistent with reports of Fe powders produced from fused salt electrolysis baths.[51] The particle size and morphology of metal powders significantly influences their sintering behavior, flow properties, and suitability for powder metallurgy applications.[52] In this case, the recovered Fe powder may be directly suitable for powder-based forming or alloying applications with minimal post-processing. Additionally, the ability to produce ferromagnetic, chloride-free Fe powder directly from industrial waste streams such as SPL provides a compelling value proposition for circular economy approaches in the steel industry. From a scalability perspective, the CMSE process benefits from high deposition rates, high coulombic efficiency, and the ability to produce high-purity metallic Fe which are key advantages for industrial implementation. While aqueous electrochemical routes are more attractive in terms of operating temperature, they are generally limited by slower kinetics and lower efficiencies due to parasitic reactions (water electrolysis). Thus, while aqueous processes may remain attractive for some applications, CMSE offers distinct advantages for large-scale, high-throughput Fe recovery.

Conclusions

This study demonstrates the feasibility and effectiveness of chloride-based molten salt electrolysis (CMSE) for recovering high-purity iron from spent pickle liquor (SPL), which is a waste byproduct of steel manufacturing. Through a combination of thermal dehydration followed by high-temperature electrolysis, SPL was successfully transformed into a valuable metallic Fe powder. The findings support the integration of CMSE into future steelmaking workflows. Specific conclusions drawn from this study are:

- Electrochemical characterization confirmed Fe^{2+} as the dominant species in SPL, enabling its direct conversion to dry $FeCl_2$ through controlled thermal dehydration under inert conditions.
- Dehydrated SPL served as an effective feedstock for CMSE, yielding dense, ferromagnetic iron deposits with high purity (99.9 wt % after arc melting).
- Coulombic efficiency above 85% was achieved in CMSE, validating the energy efficiency and process practicality advantages of the proposed feedstock valorization approach.
- Recovered iron powders exhibited favorable morphology and magnetic properties, making them potentially suitable for powder metallurgy applications, while simultaneously addressing waste management challenges in the steel industry.

Acknowledgments

This work was supported by the U.S. Department of Energy's Industrial Efficiency and Decarbonization Office under Office of Energy Efficiency and Renewable Energy, Award Number DE-EE0010846. Portions of this work were performed at LLNL under Contract Number DE-AC52-07NA2. The views expressed herein do not necessarily represent the views of the U.S. Department of Energy or the United States Government. We gratefully acknowledge Bill King and Cleveland-Cliffs Inc. for providing the spent pickle liquor samples used in this study.

ORCID

Anar Badalbayli https://orcid.org/0009-0006-4370-3322
Nicholas Sinclair https://orcid.org/0000-0002-8268-966X
Rohan Akolkar https://orcid.org/0000-0002-9865-5704

References

1. S. S. Chandel, P. K. Singh, P. K. Katiyar, and N. S. Randhawa, *Min. Metall. Explor.*, **40**, 2059 (2023).
2. T. Özdemir, C. Öztin, and N. S. Kıncal, *Chem. Eng. Commun.*, **193**, 548 (2006).
3. J. Tang, Y. Pei, Q. Hu, D. Pei, and J. Xu, *Procedia Environ. Sci.*, **31**, 778 (2016).
4. R. D. Hoak, *Ind. Eng. Chem.*, **39**, 614 (1947).
5. M. Regel-Rosocka, *J. Hazard. Mater.*, **177**, 57 (2010).
6. B. Marszałkowska, M. Regel-Rosocka, Ł. Nowak, and M. Wiśniewski, *Pol. J. Chem. Technol.*, **12**, 1 (2010).
7. A. Devi, A. Singhal, and R. Gupta, *Int. J. Environ. Sci.*, **4**, 284 (2013).
8. M. Kordloo, H. Noeparast, A. R. Ashani, M. H. Nasab, and Y. Ghorbani, *Environ. Technol. Innov.*, **36**, 103826 (2024).
9. R. Gueccia, D. Bogle, S. Randazzo, A. Tamburini, A. Cipollina, D. Winter, J. Koschikowski, and G. Micale, *Membranes*, **12**, 114 (2022).
10. A. A. Baba, A. Adekola, O. S. Awobode, B. R. Adekunle, S. Pradhan, and A. Biswal, *Int J Chem*, **21**, 231 (2011).
11. J. M. Zinck and B. C. Aube, *CIM Bull.*, **93**, 98 (2000).
12. E. Jarosz-Krzemińska, E. Helios-Rybicka, and M. Gawlicki, *Int. J. Environ. Sci. Technol.*, **12**, 2901 (2015).
13. R. D. Hoak, C. J. Lewis, C. J. Sindlinger, and B. Klein, *Ind. Eng. Chem.*, **39**, 131 (1947).
14. L. Weitzman, *J. Hazard. Mater.*, **24**, 157 (1990).
15. A. K. Minocha, N. Jain, and C. L. Verma, *Cem. Concr. Res.*, **33**, 1695 (2003).
16. M. B. Mansur, S. D. F. Rocha, F. S. Magalhães, and J. dos S. Benedetto, *J. Hazard. Mater.*, **150**, 669 (2008).
17. M. Tomaszewska, *Sep. Purif. Technol.*, **22–23**, 591 (2001).
18. J. Jandová, J. Maixner, and T. Grygar, *Ceram.-Silikáty*, **46**, 52 (2002).
19. G. Csicsovszki, T. Kékesi, and T. I. Török, *Hydrometallurgy*, **77**, 19 (2005).
20. J. Dufour, C. Negro, F. Heras, and F. López-Mateos, *ISIJ Int.*, **41**, 801 (2001).
21. M. K. Sinha, S. K. Sahu, P. Meshram, and B. D. Pandey, *Hydrometallurgy*, **147–148**, 103 (2014).
22. A. S. Ramage, (1905), https://patents.google.com/patent/US788064A/en.
23. J. R. Cain, (1934), https://patents.google.com/patent/US1954664A/en.
24. G. W. Bodamer and H. Collins, (1957), https://patents.google.com/patent/US2810686A/en.
25. R. D. Hoak, *Sew. Works J.*, **17**, 940 (1945).
26. L. Grenni, *Thesis* (1957), https://digitalcommons.njit.edu/theses/2526.
27. J. K. Seyler, W. E. Thornton, and M. K. Householder, *Sulfuric acid and Ferrous-Sulfate Recovery from Waste Pickle Liquor* (Office of Research and Development, US Environmental Protection Agency) (1974).
28. G. Huang, J. Chen, and S. Gao, *Water Air Soil Pollut.*, **231**, 389 (2020).
29. X. Gao, Y.-N. Zhou, D. Han, J. Zhou, D. Zhou, W. Tang, and J. B. Goodenough, *Joule*, **4**, 1864 (2020).
30. K. Liddell, *Hydrometallurgy*, **76**, 181 (2005).
31. S. Hu, H. Zhang, X. Tan, S. Ni, and S. Li, *Hydrometallurgy*, **224**, 106259 (2024).
32. Q. Zhao, W. Li, C. Liu, M. Jiang, H. Saxén, and R. Zevenhoven, *J. Sustain. Metall.*, **9**, 148 (2023).
33. S. Gao, J. Chen, and G. Huang, *Water Air Soil Pollut.*, **233**, 365 (2022).
34. A. Badalbayli, N. Sinclair, E. Kim, A. A. Baker, and R. Akolkar, *J. Electrochem. Soc.*, **172**, 032508 (2025).
35. B. Levich, *Discuss. Faraday Soc.*, **1**, 37 (1947).
36. M. Laliberté, *J. Chem. Eng. Data*, **52**, 321 (2007).
37. S. K. Guchhait, H. Sammi, K. K. Yadav, S. Rana, and M. Jha, *J. Mater. Sci., Mater. Electron.*, **32**, 2965 (2021).
38. A. Devi, A. Singhal, R. Gupta, and P. Panzade, *Clean Technol. Environ. Policy*, **16**, 1515 (2014).
39. D. Inman, J. C. Legey, and R. Spencer, *J. Appl. Electrochem.*, **8**, 269 (1978).
40. G. M. Haarberg, E. Kvalheim, S. Rolseth, T. Murakami, S. Pietrzyk, and S. Wang, *ECS Trans.*, **3**, 341 (2007).
41. B. Khalaghi, E. Kvalheim, M. Tokushige, L. Teng, S. Seetharaman, and G. M. Haarberg, *ECS Trans.*, **64**, 301 (2014).
42. S. Wang, G. M. Haarberg, and E. Kvalheim, *J. Iron. Steel Res. Int.*, **15**, 48 (2008).
43. S. Prabu and H. Wang, *Chin. J. Chem. Eng.*, **28**, 854 (2020).
44. P. A. Solli, T. Eggen, E. Skybakmoen, and Å. Sterten, *J. Appl. Electrochem.*, **27**, 939 (1997).
45. A. Allanore, H. Lavelaine, G. Valentin, J. P. Birat, P. Delcroix, and F. Lapicque, *Electrochim. Acta*, **55**, 4007 (2010).
46. A. Badalbayli, N. Sinclair, R. Bernasconi, N. Borisenko, K. Venkatesh, A. Ispas, R. Akolkar, and L. Magagnin, *Electrochem. Soc. Interface*, **33**, 47 (2024).
47. Y. Baoxu, C. Haixiang, and K. Dejun, *Trans. Indian Inst. Met.*, **71**, 617 (2018).
48. A. R. Moss, *J. Common Met.*, **1**, 60 (1959).
49. J. Geng, Y. Luo, H. Fu, Q. Dou, H. He, G. Ye, and Q. Li, *Prog. Nucl. Energy*, **147**, 104212 (2022).
50. L. Lu, *Iron Ore: Mineralogy, Processing and Environmental Sustainability* 2nd ed.1 (Elsevier Science & Technology, San Diego) (2021).
51. A. B. Suchkov, T. N. Ermakova, and V. B. Akimenko, *Sov. Powder Metall. Met. Ceram.*, **7**, 425 (1968).
52. W. J. Kroll, *Trans. Electrochem. Soc.*, **87**, 551 (1945).